# COMPUTATIONAL MODEL OF AN SPT-100 THRUSTER

**Justin W. Koo♦ and Iain D. Boyd+**
**Nonequilibrium Gas and Plasmadynamics Group**
**Department of Aerospace Engineering**
**University of Michigan**
**Ann Arbor, Michigan 48109**

*Abstract*

*Existing models have developed computational Hall thruster codes to a level where qualitative features of the plasma and electric field can be reproduced. These results are possible only with the use of corrections to various transport and energy parameters; however, these corrections are not rigorously defined by the actual physics governing these processes. This paper presents a 2-D hybrid PIC-MCC with an explicit electron energy formulation. The results presented focus on a particular correction factor introduced by Boeuf and Garrigues[6] which influences the electron mobility and electron energy loss rate. This correction factor, $\alpha$, is varied over a range which resembles typical thruster operation and results are presented. The model is applied to a SPT-100 Hall thruster. The electron energy profile is shown to be highly dependent on the $\alpha$ parameter through the electron energy loss rate. Finally, detailed results are presented for a specific case.*

## 1. INTRODUCTION

Experimental study of Hall thrusters has far outpaced the computational study of these devices in the decades since their introduction; however, interest remains in the development of robust, accurate, and efficient hall thruster codes. Among the numerous benefits of a computational model would be the ability to perform full spacecraft integration studies, the means to quantify chamber effects in experimental tests, and the capacity to perform virtual life tests for a fraction of the cost of actual life tests.

Many new computational models of the plasma properties inside Hall thrusters have been developed recently. They range from 1-D and 2-D steady-state models such as those by Keidar et al.[1], Ahedo et al.[2], to 2-D fluid models by Roy and Pandey[3], to full 1-D and 2-D time dependent models by Komurasaki and Arakawa[4], Fife[5], Boeuf and Garrigues[6], and, most recently, by Hagelaar et al.[7] and others. These computational models have reached a stage of refinement where, with a priori knowledge of a particular experimental flow condition, a reasonably representative computational solution can be achieved in a matter of hours.

Unfortunately, these solutions are by no means sufficiently reliable to prompt widespread use in the Hall thruster design community. In particular, although computational models can be tuned to produce plasma structures and electric fields which are qualitatively similar to results obtained from internal experimental diagnostic studies, guaranteeing fidelity over a wide range of operating conditions is not yet feasible. Unreliable accuracy can be attributed to many factors including the dependence on loosely based empirical corrections for the electron mobility and energy-loss rates and the global use of a thermalized potential in the field calculation.

♦ Graduate Student, kooj@engin.umich.edu
+ Professor, Department of Aerospace Engineering

The model presented in this paper is a continuation of previous work by Koo et al.[8]. The principal update is the substitution of an implicit electron energy equation with an explicit electron energy equation similar to that used by Fife[5].

## 2. COMPUTATIONAL MODEL

This model provides a 2-D axisymmetric hybrid PIC-MCC description of the acceleration channel and near-field of a SPT-type Hall thruster. It is based on a quasineutral plasma description where heavy particles (Xe, $Xe^+$) are treated with a PIC-MCC model. The electron fluid is modeled with a 1-D electron energy model. Plasma potential is calculated using a 1-D Ohm's Law formulation.

The geometry considered in this model covers from the anode to 3.5 cm past the exit plane of the thruster in the axial direction and from the thruster centerline to 2 cm past the outer channel diameter in the radial direction. The magnetic field configuration tested represents an SPT-100 thruster. The magnetic field is calculated using a Poisson solver ($\nabla^2 B = 0$) with boundary conditions derived from experimental sources. The magnetic field configuration is shown in Fig. 1.

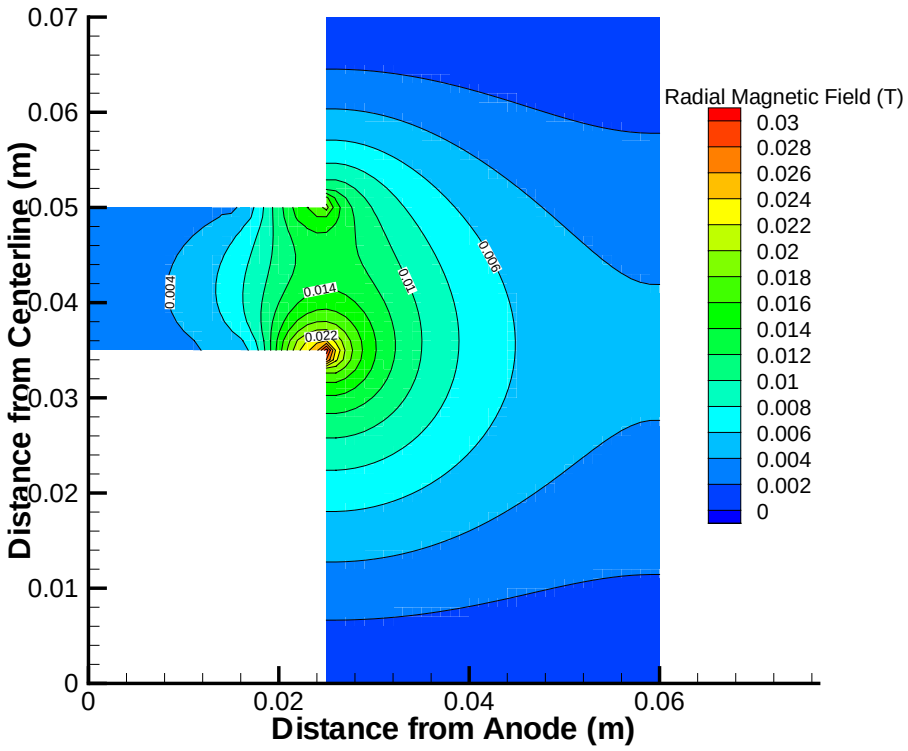


Figure 1: Radial Magnetic Field Configuration

The magnetic field configuration is used to calculate the magnetic field streamfunction via the following relations:

$$\frac{\partial \lambda}{\partial r} = rB_z \qquad \frac{\partial \lambda}{\partial z} = -rB_r$$

Equipotentials of the streamfunction correspond to magnetic field lines and are used to formulate the 1-D Ohm's Law and 1-D electron energy equations. The magnetic field lines are shown in Fig 2.

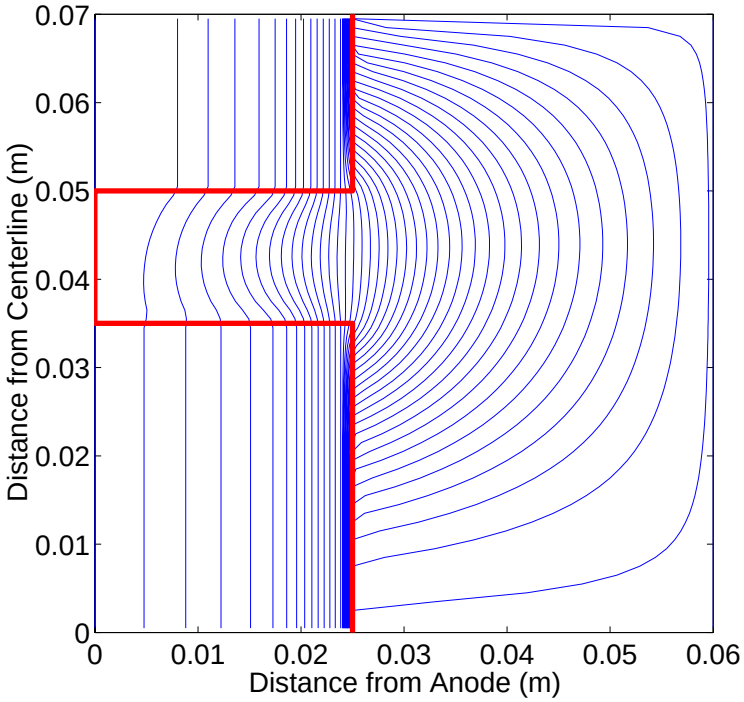


Figure 2: Magnetic Field Lines

The normal derivative with respect to field lines can be written as follows:

$$\frac{\partial}{\partial \hat{n}} = rB\frac{\partial}{\partial \lambda}$$

A fundamental premise of the reduction of this 2-D problem into a 1-D Ohm's Law formulation is the idea that there is a constant defined for each individual field line which is a balance between the electrostatic pressure and the electron thermal pressure along field lines. This concept, first introduced by Morozov[9], is known as the thermalized potential and is defined as follows:

$$\phi^*(\lambda) = \phi(\lambda) - \frac{kT_e}{e}\ln\left(\frac{n}{n^*}\right)$$

where n* is an arbitrary constant. Thus, along a given field line, the potential and density vary such as to maintain a constant thermalized potential while from a given field line to a different field line, the value of the thermalized potential may vary.

Only singly charged xenon particles are considered in this model. The source term for $Xe^+$ is as follows:

$$\frac{\partial n_i}{\partial t} = n_i n_a \nu_{ionization}(\varepsilon)$$

where the right hand side consists of the plasma density, neutral density, and ionization rate, respectively. The ionization rate is based on tabulated ion-neutral ionization rates reported by Puech and Mizzi[10].

Neutrals are injected at the anode to match the desired mass flow rate (between 4 and 5 mg/s). They are removed from the simulation via a Monte-Carlo Collision (MCC) model at the same rate as the creation of $Xe^+$. Newly ionized $Xe^+$ particles are born with a Maxwellian velocity distribution based on a 1000 K reference temperature.

Wall recombination occurs when ions strike any thruster wall and results in the formation of an equal number of fully accommodated (1000 K) neutral particles. Neutral scattering at the wall is also based on full thermal accommodation.

The motion of the heavy particles is based on a first order advection scheme. New ion velocities are calculated from the electrostatic field equations at half-steps relative to ion positions. Quantities update in the same manner as a classical leapfrog update scheme.

$$u^{t+\frac{\Delta t}{2}} = u^{t-\frac{\Delta t}{2}} + \frac{eE}{m}\Delta t$$

$$x^{t+\Delta t} = x^{t} + u^{t+\frac{\Delta t}{2}}\Delta t$$

Electrons are assumed to be isothermal along magnetic field lines. This allows the 1-D decomposition of the electron energy equation across field lines. The complete electron energy equation is as follows:

$$\frac{\partial}{\partial t}\left(n_e\varepsilon\right) + \vec{\nabla}\bullet\left[\frac{5}{3}n_e\varepsilon\vec{u}_e - \frac{10}{9}n_e\mu_e\varepsilon\vec{\nabla}\varepsilon\right] = -n_e\vec{u}_e\bullet\vec{E} - n_e\varepsilon\nu_{loss}(\varepsilon)$$

where the electron loss frequency is defined as:

$$\nu_{loss}(\varepsilon) = \nu_{e-n}(n_a,\varepsilon) + \nu_{walls}(\varepsilon)$$

The first term composing the loss frequency is the frequency of ionization energy losses and the second term is a wall-loss term. The form chosen for this wall-loss term , as suggested by Boeuf and Garrigues[6], is:

$$\nu_{walls}(\varepsilon) = \alpha * 10^7 \exp\left(\frac{-20}{\varepsilon}\right)$$

The dependence of the solution on the α parameter will be presented in this paper. The electron energy is fixed at 3 eV at the anode and 2 eV at the domain exit.

The electron energy equation above can be recast in the form of an ordinary differential equation with a dependence on the electron energy alone. Volume integration of the electron energy equation is used to evaluate the coefficients in a smooth manner. Stable integration of the resulting ODE requires a timestep far smaller than the timestep used for heavy particle evolution. As suggested by Fife, the electron energy equation is subcycled 100 times for every single heavy particle timestep to ensure accurate integration.

The transverse magnetic field electron mobility is needed for calculation of the electrostatic field. To ensure that the electron mobility does not drop catastrophically in regions of neutral depletion, the electron momentum transfer frequency is supplement by an effective wall scattering term also suggested by Boeuf and Garrigues[6]. This leads to the following term for the electron momentum transfer frequency:

$$\nu_{mom} = \nu_{neutrals} + \nu_{walls}$$

Where,

$$\nu_{neutrals} = 2.5 * 10^{-7} n_a \qquad \nu_{walls} = \alpha * 10^7$$

This effective momentum transfer frequency is used in the classical description of the transverse magnetic field electron mobility:

$$\mu_e = \frac{e}{m\nu_{mom}} \frac{1}{1+\left(\frac{\omega_e}{\nu_{mom}}\right)^2}$$

Where $\omega_e$ is the electron cyclotron frequency.

The electrostatic field calculation is based on a 1-D Ohm's Law formulation ensuring that there is no net buildup of charge. This requires the sum of the electron and ion currents to balance throughout the domain as follows:

$$I_T = \int_S j_e \partial S + \int_S j_i \partial S = \int_S en_e \mu_e rB \left( -\frac{\partial \phi^*}{\partial \lambda} - \left[ \ln\left(\frac{n_e}{n^*}\right) - 1 \right] \frac{k}{e} \frac{\partial T_e}{\partial \lambda} \right) \partial S + \int_S en_i u_i \partial S$$

This equation is summed from the anode to the cathode and the following closed form solution for the total current can be derived:

$$I_T = \frac{-\Delta\phi^* - \sum \frac{\int_S en_e \mu_e rB \left[ \ln\left(\frac{n_e}{n^*}\right) - 1 \right] \frac{k}{e} \frac{\partial T_e}{\partial \lambda} \partial S}{\int_S en_e \mu_e rB \partial S} d\lambda + \sum \frac{\int_S en_i u_i \partial S}{\int_S en_e \mu_e rB \partial S} d\lambda}{\sum \frac{1}{\int_S en_e \mu_e rB \partial S} d\lambda}$$

Once the total current is known, the derivative of the thermalized potential can be calculated directly and a full 1-D potential can be constructed. The potential is then calculated along field lines through the use of the thermalized potential and then extrapolated through the whole domain.

The computational model is compiled with SUN f77 to run on a Sun Ultra 10/440 MHz workstation. A simulation typically contains 60,000 ion macroparticles and 60,000 neutral macroparticles. The heavy particle timestep is limited to the time needed for a perfectly accelerated particle to cross half a computional cell which results in a timestep of about $2.5 \times 10^{-8}$ seconds. A typical solution time is 8 hours.

## 3. RESULTS AND DISCUSSION

The primary focus of the present study is on the effect of the $\alpha$ parameter on this model. This parameter, proposed by Boeuf and Garrigues[6], is used for two functions. First, it increases the electron momentum transfer frequency to ensure that the mobility does not drop catastrophically in regions of neutral depletion, and second, it represents an energy loss term to the channel walls and thus acts as an energy sink. This leads to an interpretation of the $\alpha$ parameter as simulating secondary electron emission.

Simulations are run for identical flow conditions with variation of $\alpha$ from 0.20 to 0.05. Four equally spaced conditions (0.20, 0.15, 0.10 and 0.05) are shown in a series of plots comparing plasma potential, electron energy, and plasma density. A fifth condition (0.11) is studied in more detail later on in this section.

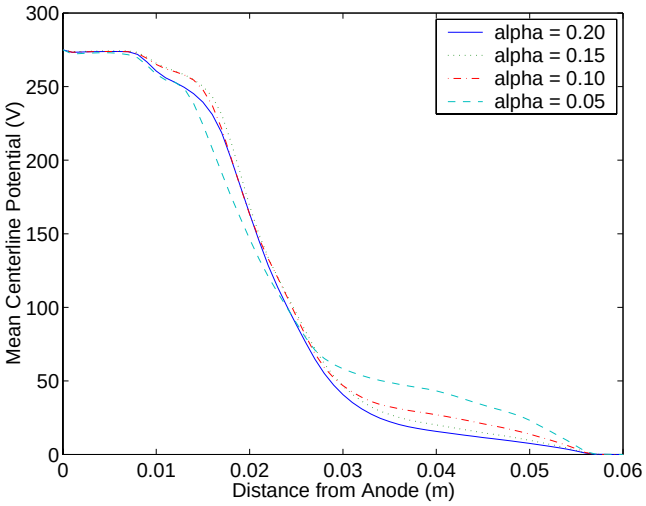


Figure 3: Mean Centerline Potential

As shown in Fig. 3, the effect of α on the centerline potential is relatively small. As can be seen above, decreasing the value of α results in a marginally steeper potential gradient; however, the potential drop remains centered roughly 2.0 cm from the anode. A lower α also results in a slightly higher plume potential.

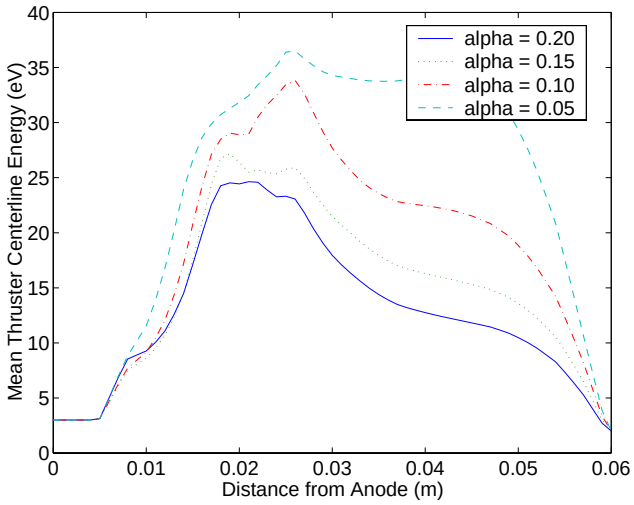


Figure 4: Mean Centerline Electron Energy

As shown in Fig. 4, there is a strong effect of the α parameter on the centerline electron energy profiles. As expected, the larger α values lead to a much lower energy peak. In addition, the high α values seem to shift the energy curve towards the anode. There is also strong dependence on α in the near field plume. The higher α values in the plume lead to lower electron energy in that region. Although the magnitude of the plume energy is quite large, especially for the low α cases, the neutral and plasma densities are low enough that the primary ionization zone remains inside the thruster.

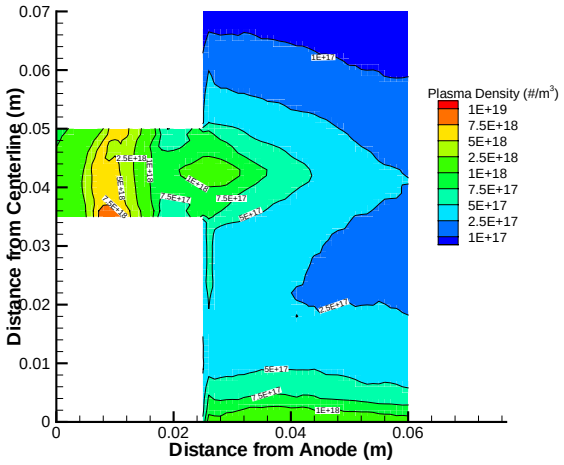


Figure 5: Mean Plasma Density $\alpha = 0.05$

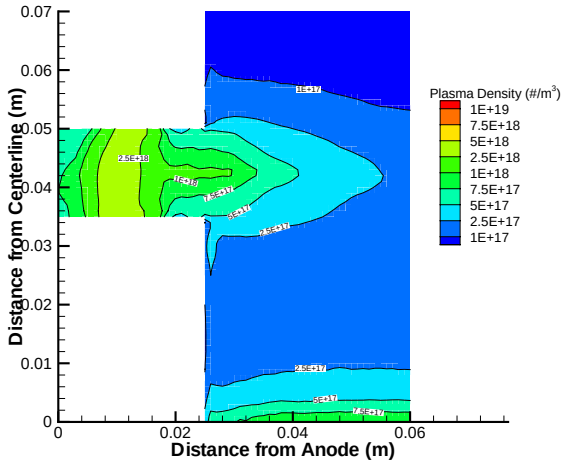


Figure 6: Mean Plasma Density $\alpha = 0.10$

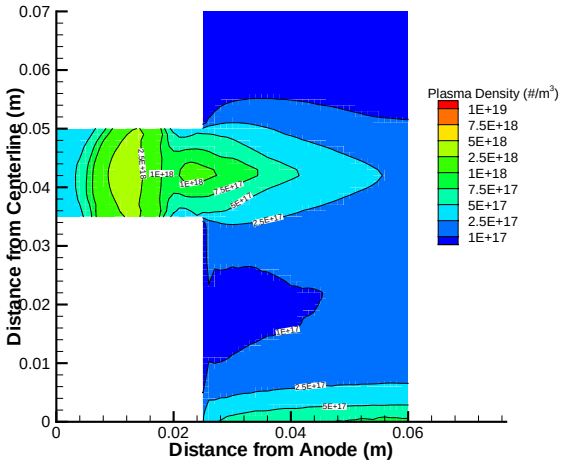


Figure 7: Mean Plasma Density $\alpha = 0.15$

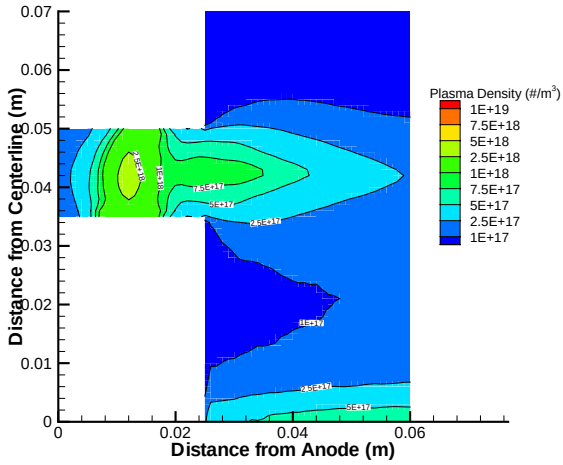


Figure 8: Mean Plasma Density $\alpha = 0.20$

The magnitude of the mean plasma densities above are strongly correlated with the electron energies shown in Fig. 4. As expected, with a high $\alpha$ parameter, a lower peak plasma density is observed. The "pinching" of the plasma plume around the exit plane of the thruster, which is especially evident in Fig. 5 and Fig. 7, is due to the focusing effect of the magnetic field geometry used in this simulation. In addition, there is a bias towards higher plasma density towards the inner wall of the thruster. A small pocket of high density plasma can be seen in the low $\alpha$ case, Fig. 5, while it does not seem as prominent in the low $\alpha$ cases, Fig. 6-8.

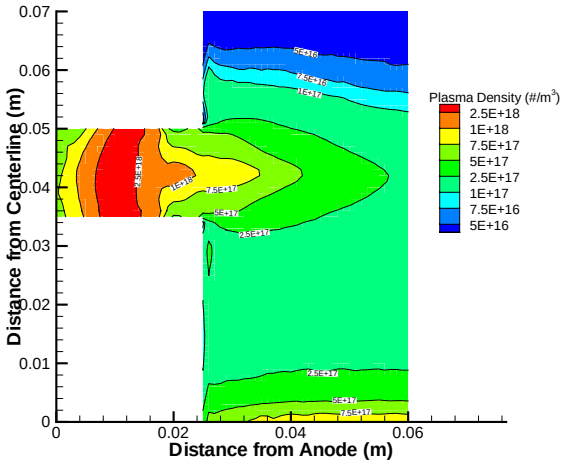


Figure 9: Mean Plasma Density $\alpha = 0.11$

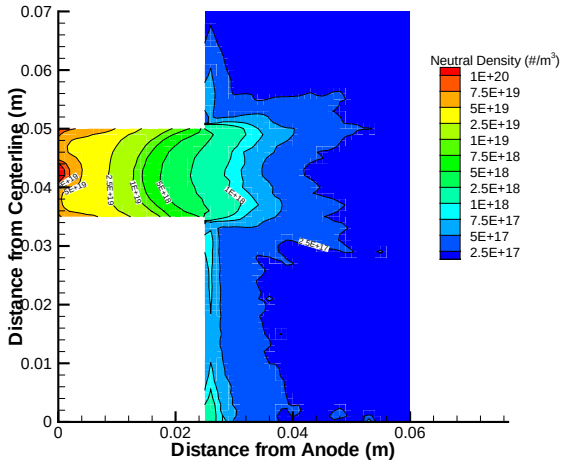


Figure 10: Mean Neutral Density $\alpha = 0.11$

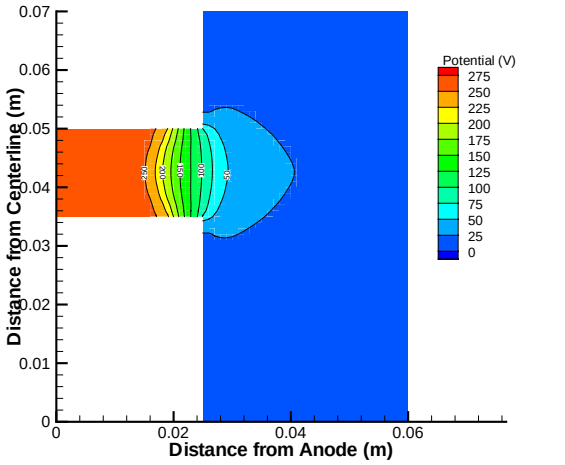


Figure 11: Mean Potential $\alpha = 0.11$

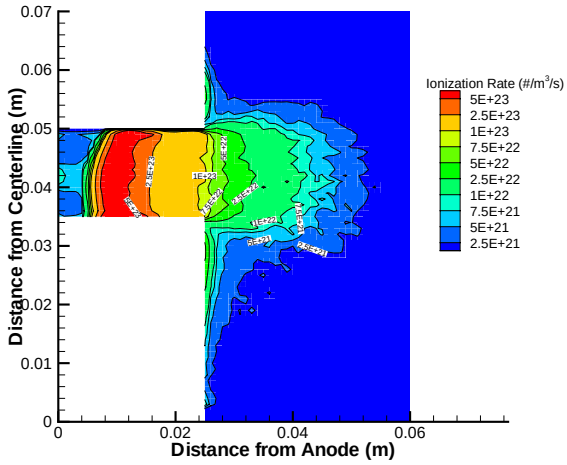


Figure 12: Mean Ionization Rate $\alpha = 0.11$

Finally, the case of $\alpha$ equal to 0.11 is chosen to provide a more detailed view of the plasma structure. The mean plasma density appears in Fig. 9 and shows a peak plasma density approximately equal to that computed by Hagelaar et al.[7] for a SPT-100 thruster. The mean neutral density in Fig. 10 also shows some similarity with the shape observed by Hagelaar et al.[7]. Although an additional mobility correction was used by Hagelaar et al.[7], even the shape of the potential distribution remains similar, as shown in Fig. 11. The biggest difference between this model and that of Hagelaar et al[7] is evident in Fig. 12. For this model, the peak source regions extends all the way from the inner to the outer wall of the thruster. The location of these high ionization regions all the way to the wall is strongly dependent on the high local neutral densities due to wall recombination. Finally the magnitude of even these peak ionization regions is, at best, half that of the peak ionization regions observed by Hagelaar et al.[7].

## 4. SUMMARY AND FUTURE WORK

This paper demonstrates the strong dependence of this model on a particular tunable parameter in the electron mobility and electron energy loss frequency. Clearly, there is a strong linkage between the electron energy and the parameter $\alpha$ with a higher $\alpha$ being associated with a lower peak electron energy profile. The correlation between the potential and the parameter $\alpha$ is significantly weaker with a lower $\alpha$ being

associated with a marginally steeper potential gradient. The location and magnitude of the plasma is highly dependent on the electron energy and thus also shows a strong dependence on $\alpha$.

Future plans call for the development of an improved electron energy model, possibly through the use of either a non-local approximation or a full 2-D electron energy equation. Corresponding changes to the potential calculation must also be included. In addition, $Xe^{++}$ tracking and improved wall/sheath models must be developed if further gains in accuracy are desired. Along with development of the computational model, extensive comparison with existing experimental data for the SPT-100 as well as with the UM/AFRL P5 is also planned.

## 5. ACKNOWLEDGEMENTS

The first author gratefully acknowledges financial support from the Department of Energy through a Computational Science Graduate Fellowship and a University of Michigan Rackham Travel Fellowship.

---

[1] Keidar, M., Boyd, I.D., and Beilis, I.I., "Plasma Flow and Plasma-Wall Transition in Hall Thruster Channel," *Physics of Plasmas*, Vol. 9, 2002, pp. 5315-5322.

[2] Ahedo, E., Martinez-Cerezo, P., and Martinez-Sanchez, M., "One-Dimensional Model of the Plasma Flow in a Hall Thruster," *Physics of Plasmas*, Vol. 8, 2001, pp. 3058-3068.

[3] Roy, S. and Pandey, B.P., "Numerical investigation of a Hall thruster plasma", *Physics of Plasmas*, Vol. 9, 2002, pp. 4052-4060.

[4] Komurasaki, K. and Arakawa, Y., "Two-Dimensional Numerical Model of a Plasma Flow in a Hall Thruster," *Journal of Propulsion and Power*, Vol. 11, 1995, pp. 1317-1323.

[5] Fife, J.M., "Hybrid-PIC Modeling and Electrostatic Probe Survey of Hall Thrusters," Doctoral Thesis, Massachusetts Institute of Technology, Department of Aeronautics and Astronautics, September 1998.

[6] Boeuf, J.-P. and Garrigues, L., "Low Frequency Oscillations In a Stationary Plasma Thruster," *Journal of Applied Physics*, Vol. 84, 1998, pp. 3541-3544.

[7] Hagelaar, G. J. M., Bareilles, J., Garrigues, L., and Boeuf, J.-P., "Two-dimensional model of a stationary plasma thruster," *Journal of Applied Physics*, Vol. 91, 2002, pp.5592-5598.

[8] Koo, J. W., Boyd, I. D., Haas, J. M., Gallimore, A. D., "Computation of the Interior and Near-Field Flow of a 2-kW Class Hall Thruster," AIAA-2001-3321, 37th Joint Propulsion Conference, Salt Lake City, UT, 2001.

[9] Morozov, A. I., Esipchuk, Yu. V., Tilinin, G. N., Trofimov, A. V., Sharov, Yu. A., Shchepkin, G. Ya., "Plasma Accelerator With Closed Electron Drift and Extended Acceleration Zone," *Soviet Journal of Plasma Physics*, Vol. 17, 1972, p.38.

[10] Puech V. and Mizzi, S., "Collision cross sections and transport parameters in neon and xenon" *, Journal of Physics D*, 1991, p. 1974-1985.